

Cite this: *RSC Adv.*, 2018, **8**, 37085

In situ investigation of the kinetics and microstructure during photopolymerization by positron annihilation technique and NIR-photorheology[†]

Helena Švajdlenková, ^a Ondrej Šauša, ^b Gernot Peer^{cd} and Christian Gorsche

The microstructural free volume evolution during a photopolymerization process was studied on a commercial photopolymer (SPOT LV) *in situ* by positron annihilation lifetime spectroscopy (PALS) and concomitant NIR-photorheology. Analysis of the positron lifetime spectra revealed a high sensitivity of the PALS technique to the different phases of photopolymerization associated with different reaction rates as well as to the evolution of microstructural free-volume shrinkage, which was described at the molecular level by the Kohlrausch–Williams–Watts equation. The *in situ* PALS study of microstructural changes in photopolymerization was related to the vitrification (gel point) accompanied by shrinkage stress registered *via* NIR-photorheology. The simultaneous NIR measurements yield information on the monomer conversion of SPOT LV, which can be correlated to the occurrence of the gel point and the evolution of the microstructural free volume. This combined study allows us to see deeper into the crosslinking process and its influence on the resulting material characteristics.

Received 11th September 2018
Accepted 29th October 2018

DOI: 10.1039/c8ra07578f

rsc.li/rsc-advances

1. Introduction

Photopolymerization is an efficient technique for the rapid production of thermosets with low energy consumption and unprecedented physical and mechanical properties. One of its advantages is the possibility to modify the material properties for a wide variety of applications, such as protective and decorative coatings,¹ dental medicine² and 3D-printing.³ The process of photopolymerization is a very complex phenomenon, which has been studied very intensively using different techniques. The most extensively studied factors are the compound composition, the curing conditions (*e.g.* the time, wavelength spectrum and intensity of radiation, reaction temperature), and macroscopic physical and mechanical properties of the final materials. It is possible to investigate the curing process, accompanied by volume reduction, *via* photo-DSC,⁴ and photodilatometry.^{5,6} Another suitable method for studying photopolymerization is real-time infrared spectroscopy (RT-IR) due to its continuous and exact

determination of the rate of reaction and the conversion of monomers.^{7,8} An important and versatile tool for the *in situ* characterization of photopolymerization reactions is the simultaneous combination of techniques, for instance, real-time near-/mid-infrared (NIR/MIR)-photorheology.⁹ The coupled photorheometry with NIR spectroscopy simultaneously provides molecular information, such as double bond conversion (DBC) and shrinkage stress data.^{9,10} In addition, NIR-ultrasonic reflectometry,¹¹ dynamic shrinkage measurement with NIR spectroscopy¹² or the dielectric spectroscopy (DS) also appears to be a suitable technique for the monitoring of photopolymerization.^{13,14} Each of these techniques contribute to our knowledge of both, the crosslinking process and the resulting properties of materials.

One of the most important factors studied is shrinkage stress, a long-term problem influencing the practical use of photopolymers, which also contributes to the increased brittleness of materials.¹⁵ The negative impact of shrinkage and shrinkage stress on the material properties has been mainly studied in dental resins.^{16,17} It is known that the crosslinking process for (meth)acrylates proceeds very fast and inhomogeneously, yielding incomplete conversion of monomers. A very promising direction is regulated photopolymerization using chain transfer agents such as thiols¹⁸ or addition–fragmentation chain transfer agents (AFCTs).¹⁹ Employing such chemistry leads to a more homogeneous crosslinking reaction obtaining materials with tailored network architecture, thus reduced shrinkage stress and high toughness.^{20,21}

^aPolymer Institute of SAS, Dúbravská cesta 9, 845 41 Bratislava, Slovakia. E-mail: helena.svajdlenkova@savba.sk

^bInstitute of Physics of SAS, Dúbravská cesta 9, 845 11 Bratislava, Slovakia

^cInstitute of Applied Synthetic Chemistry, TU Wien, Getreidemarkt 9/163 MC, 1060 Vienna, Austria

^dChristian-Doppler-Laboratory for Photopolymers in Digital and Restorative Dentistry, Getreidemarkt 9, 1060 Vienna, Austria

† Electronic supplementary information (ESI) available. See DOI: [10.1039/c8ra07578f](https://doi.org/10.1039/c8ra07578f)



As outlined above, many studies focus on the macroscopic properties of photopolymers but a deeper view into the microstructure of cured samples is limited. In recent decades, the PALS technique has also begun to be used in the study of free volume microstructures in photopolymers.²² This technique measures the lifetime of positrons injected into the investigated material. Part of the positrons can create a bound state with an electron, called a positronium (Ps), whose triplet state, *ortho*-positronium (*o*-Ps) as a local electron density probe, is trapped in the local free volume (e.g. cavities, pores). The *o*-Ps is annihilated by the electrons from the wall of the cavity and this mode of annihilation is called a pick-off annihilation, which is dominant for the material with short lifetimes (shorter than a few ns). The three gamma annihilation as a competitive process is in this case negligible. The “*o*-Ps lifetime” used in the text means the lifetime of *o*-Ps annihilated *via* pick-off process. The average lifetime of *o*-Ps, $\tau_{\text{o-Ps}}$, depends on the dimension of the cavity. Using a suitable model, we can determine the size of a cavity. The technique is relatively simple and non-destructive. It is a useful tool for exploring the microstructural free volume in the range of 0.2–50 nm and the dynamics of processes in the free volume, which brings new insights into the material properties of polymers.

Our first pilot PALS study on both pure and regulated (using chain transfer agents) dimethacrylate-based networks combined a dynamic mechanical thermal analysis (DMTA), calculation of bulk density and PALS experiments. It was found that the reduced shrinkage stress in the modified networks led to closer packing, higher bulk density and smaller voids with a narrow void size distribution.²³ Next, their microstructure (of CTA-based formulations) in terms of cooperative length, relaxation, thermal macro and micro expansion and free volume characteristics below and above T_g were elucidated.²⁴

It is essential to investigate the crosslinking process more in detail, *i.e.* factors which influence network formation, as well as the final properties of materials. An *in situ* investigation of photopolymerization offers a closer look at occurring events as they take place and this can play a crucial role in the understanding of final material properties.

Previously, physical changes in slow processes, such as solidification/crystallization in polymers and in low molecular materials were very well characterized by annihilation parameters, mostly in the *o*-Ps lifetime parameter.²⁵ In addition, changes in the free volume during the recovery process in shape memory polymers,²⁶ in mechanically deformed elastomers²⁷ and the positronium formation on trapped excess electrons and radical formation at the irradiation of polymers^{28–30} are well-studied issues. In the case of time-dependent studies, annihilation parameters show changes in the physical and chemical aging/degradation of polymers,³¹ in the post curing of the epoxy resin system,³² as well as in the discontinuous investigation of cured processes *ex situ*.^{33–35} For the first time, in our work, the *in situ* time evolution of microstructural shrinkage during photopolymerization was shown by PALS technique and related to parallel NIR-photorheology measurements giving output on macrostructural changes. Also, the kinetics of photopolymerization were described *via* the free-volume concept.

2. Experimental

2.1. Materials

The commercially available resin SPOT LV, produced by Sonnaya Ulitka S.L., division Spot-A Materials was used. The mixture consists of three types of acrylates: a cycloaliphatic monofunctional acrylate (10–20 wt%), an aliphatic diacrylate (10–30 wt%), and an aliphatic triacrylate (60–80 wt%), some of which were ethoxylated. The molecular weight of the components was 190–430 g mol^{−1} and the photoinitiator was a type of phosphine oxide (1.5 wt%). More information about this resin is available on the website.³⁶

2.2. PALS experiment

2.2.1. Specification of light source. The flat violet LED OSV5YL57E1A with a maximum photon emission at 405 nm were used for illumination of the sample in an aluminium container by lightguide with 3 mm diameter. The flux density of the light on the side of the open empty aluminum container in the central part was 0.27 mW cm^{−2} measured by a PM100D – Compact Power and Energy Meter Console, with a 50 mW detector, from Thorlabs. In the experiment, the light source was fixed on the top of the chamber. The real average light intensity in bulk sample was evidently reduced compared to the thin specimen in rheometry due to scattering and light absorption. Irradiation periods in the early stadium of crosslinking were 6 s, later 60 s and then started continuous irradiation of the sample. The aluminium chamber with the light source is shown in the Fig. S1 of ESI.†

2.2.2. The positron radionuclide source. ²²Na, with 3 MBq activity and the form of NaCl salt was placed between two thin Kapton films (8 µm). The sample was injected into two identical aluminum containers with the cavity diameter of 16 mm and the cavity thickness of 3 mm covered with a Kapton foil window on the source site. A positron source, which formed a sandwich configuration, was placed between them to ensure maximal absorption of positrons by the sample.

In both containers, holes for the LEDs were made. The geometry and the intensity of the irradiation of the samples were identical for both containers. The sandwich assembly of samples is shown in the Fig. S2 of ESI.†

The positron lifetime measurements were performed by the fast–fast type of coincidence spectrometer with a time resolution of about 350 ps (full width at half of the maximum of the time instrumental curve). The time-resolving function and the correction for the annihilation in the positron source was performed by the defect-free pure Al sample. The lifetime spectra were evaluated using an LT program³⁷ and decomposed into three discrete lifetime components or two discrete and one largest continuous components by the complex mode of data evaluation. This means that the ratio of relative intensities I_1 and I_3 was fixed at 1 : 3 and the lifetime τ_1 was set at 125 ps. More information about the lifetime distribution is given in the ESI.† The first two short components were connected with the annihilation of *para*-positronium (*p*-Ps, singlet state of Ps) and the direct electron-positron annihilation in the bulk sample.



The longest-lived component from the annihilation of *o*-Ps corresponds to the average void size in a network structure, determined as follows:

The Tao-Eldrup's equation^{38,39} for the estimation of the microstructural free volume in the photopolymer was applied. This commonly used equation assumes that a positronium is trapped in the spherical free-volume holes of the polymers. The *o*-Ps lifetime $\tau_{o\text{-Ps}}$ is related to the radius r_h of a free-volume hole in eqn (1):

$$\tau_{o\text{-Ps}} = 0.5 \left\{ 1 - \frac{r_h}{(r_h + \Delta R)} + \frac{1}{2\pi} \sin \left[\frac{2\pi r_h}{(r_h + \Delta R)} \right] \right\}^{-1} \quad (1)$$

where the empirical parameter $\Delta R = 0.166$ nm was determined from the calibration of the known free-volume material data.⁴⁰ The corresponding hole volume of spherical geometry is given by eqn (2):

$$V_h = \frac{4}{3} \pi r_h^3 \quad (2)$$

We have to note that this approach of the free volume evaluation is a great simplification of the real state in specific materials with the complicated shape of voids and their dynamics. However, such approximation for the description of the photopolymerization dynamics is appropriate for this case.

2.3. NIR-photorheology

The NIR-photorheology measurements were performed on an Anton Paar MCR 302 WESP with a P-PTD 200/GL Peltier glass plate and a disposable PP25 measuring system, which is hyphenated with a Bruker Vertex 80 FTIR spectrometer, equipped with NIR optics. A detailed description on the experimental set-up and the underlying method can be found in literature.⁹ For each measurement 150 μL of sample was applied between the glass and steel parallel plates at 20 °C with a gap of 200 μm . The formulations were oscillated with a strain of 1% and a frequency of 1 Hz. As UV light source an Exfo OmniCure LX 400 spot curing system was used and the light was projected *via* a dual-waveguide onto the glass plate with the sample (LED with 400 nm, 0.05 mW cm^{-2} on the surface of the sample). During the experimental run, the storage modulus, loss modulus and normal force were measured *via* rheology. From NIR data collected during the measurements the double bond conversion (DBC) of the acrylate double bonds can be obtained *in situ*. The data were collected for 65 s in the dark and then during interrupted irradiation of the sample consisting of intervals with 6 s light impulses and 30 s periods in the dark. The data from the end of the 30 s intervals were plotted into a graph.

3. Results and discussion

3.1. PALS experiment in dark

In the first step, the influence of the radioactive source on the crosslinking process was tested. The sample was measured in the dark for 7 d at a temperature of 298 K.

These long-term measurements did not show a significant change in the *o*-Ps lifetime, $\tau_{o\text{-Ps}}$, over time (Fig. 1). This

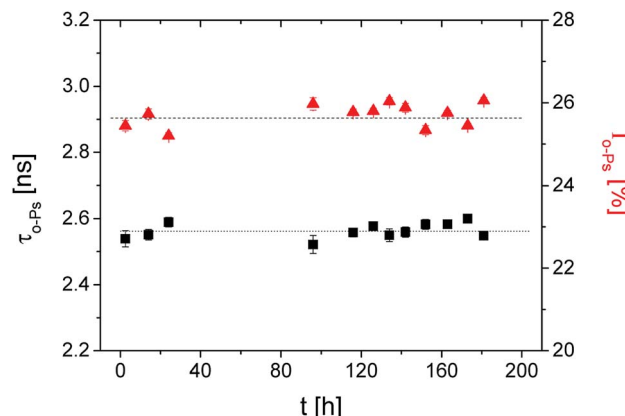


Fig. 1 The *ortho*-positronium lifetime $\tau_{o\text{-Ps}}$ (■) and the relative intensity $I_{o\text{-Ps}}$ (▲) of the sample in the dark over 7 d.

confirms that the radiation energy from the positron source does not initiate the polymerization, thus an influence during the irradiation periods of the sample by LED diodes can be excluded.

3.2. PALS measurements of the irradiated sample

It is known that the network formation during photopolymerization proceeds very fast, commonly within a few seconds (<5 s). However, a minimum one-hour-long PALS measurement for each data point was required to achieve a reasonable error in the evaluation of the lifetime spectrum. Therefore, the PALS experiment had to be performed with discontinuous irradiation of the sample by the LEDs. In addition, the low intensity of the light source slowed the photopolymerization. The flux density value of 0.27 mW cm^{-2} specified in the light source characterization above for the PALS sample container, measured at air, seems to be high. In fact, the average light intensity in the real thick bulk sample due to the different geometry of the measurement, sample size as well as the location of light guide specified in PALS experiment was substantially reduced compared to the thin sample in the rheological measurements. The optimization of the light source and chamber for PALS experiments is one of the objectives for further research.

Both factors, low intensity and discontinuous irradiation of the sample, allow to detect fine changes within the forming microstructure during the crosslinking polymerization process.

After each defined short irradiation period (6 s), the measurement of lifetimes took place in the dark for several hours, to achieve a sufficient number of annihilation events. Eight shorter (6 s) and three longer irradiation periods (60 s) were used then the continuous irradiation was followed. The accumulated (total) irradiation time is shown on the x axis.

In the first dark experiment, the total count number (tcn) for PALS spectra was about 4 M (million) where the sum of several spectra was used. Ten for PALS spectra was varied in the sample irradiation experiment. But tcn in the discontinuous irradiation was minimal at the level of 0.5 M, except for two spectra during the change to the continuous irradiation. At the end of the



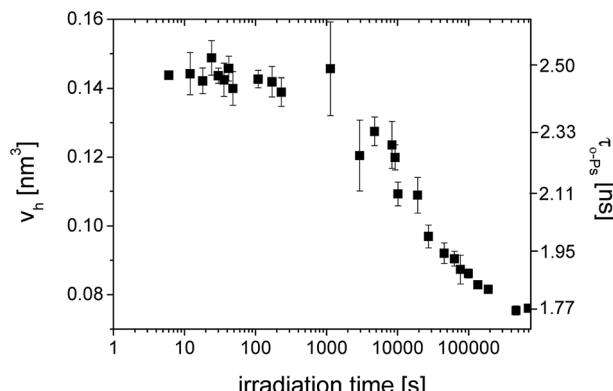


Fig. 2 The *o*-Ps lifetime, $\tau_{o\text{-Ps}}$ (■) and the calculated microstructural free volume V_h (left scale) (■) versus irradiation time during photopolymerization of SPOT LV.

photopolymerization reaction, without obvious changes in response, a large number of spectra were summed.

3.2.1. The *o*-Ps lifetime analysis. We used the continuous *o*-Ps component at the evaluation of lifetime spectra by LT program during the study of photopolymerization. The variance of fit for the evaluated spectra was better than at discrete components and this approach also provided the additional information about the homogeneity of the material structure.

In Fig. 2, we can see the irradiation time evolution of the average microstructural free volume of a network structure *via* two parameters of an *o*-Ps lifetime component, *i.e.* $\tau_{o\text{-Ps}}$, and V_h , calculated by eqn (1) and (2), respectively. Detection of microstructural shrinkage, which directly affects the strength of a material, was observed *in situ* by positron annihilation technique. The shrinkage and shrinkage stress observed during the crosslinking is due to the shortening of chemical bonds.

Larger errors at two points above 1000 s were caused by a lower total count of impulses in spectra as a result of the switching to the continuous mode of irradiation and the shorter measured time period. In this case, the sum of spectra was not appropriate.

From the literature, it is known that the evolution of a macroscopic shrinkage can be described by the Kohlrausch-Williams-Watts equation (KWW):⁴¹

$$\Delta V/V_0 = 1 - \exp(t/\tau) \quad (3)$$

where the stretched-exponent β reflects the shrinkage, ΔV is the change in the molar volume, and V_0 is the molar volume of the monomer. Fig. 3 shows the time dependence of a relative change of V_h , $(V_{hL} - V_h(t))/(V_{hL} - V_{hs})$ normalized to 1 where the constants V_{hL} and V_{hs} are the averaged values of V_h in the uncured and in the cured final sample, respectively. From the KWW fit, two parameters were obtained: the overall time-constant $\tau = 29\ 372$ s and the stretch exponent $\beta = 0.635$.

It has to be noted that the Tao-Eldrup equation (eqn (2)) is commonly used for solid and viscous materials, *e.g.* glasses. However, in the case of a liquid state, such as the uncured mixture of monomers, the bubble effect occurs at the formation of a Ps.^{22,42,43} The zero point motion of Ps creates bubble,

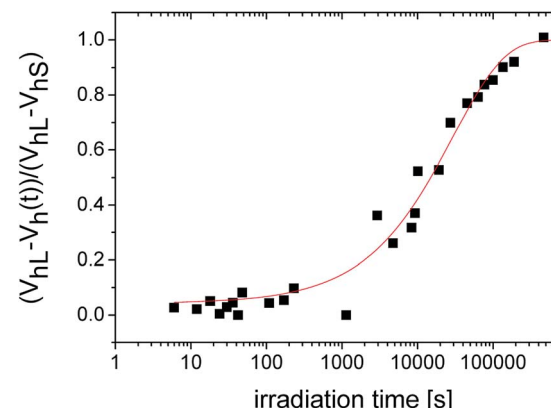


Fig. 3 The relative change of the microstructural free volume described by the KWW equation with two characteristic parameters, *i.e.* the overall time-constant $\tau = 29\ 372$ s and the stretch exponent $\beta = 0.635$.

a spherical cavity around himself whereupon the free volume “seen” by the positrons is greater than the real intermolecular space in liquids measured by other methods such as the sound velocity.⁴⁴ Therefore, the free volume determined by PALS measurements in the early stages of network formation deviates from the actual value. After the initiation of the network formation and the densification of the structure, it is expected that the V_h values are correct in the framework of the selected model for the free-volume calculation. However, this fact does not diminish the usefulness of the PALS technique for the investigation of photopolymerization reactions.

Here it is also necessary to note that the common used value of the empirical parameter $\Delta R = 0.166$ nm can vary for different types of matter. For instance some measurements showed^{45,46} that smaller value of ΔR (about 0.15 nm) should be more suitable for polymers. In this work we used the simple approach and the value $\Delta R = 0.166$ nm. It would be interesting in the future to clarify the question of an appropriate value of ΔR for this type of material.

3.2.2. Analysis of the intensity of *o*-Ps component, $I_{o\text{-Ps}}$. The second most important quantity in this PALS study is the relative intensity, $I_{o\text{-Ps}}$. The $I_{o\text{-Ps}}$ is connected with the probability of Ps formation in the material and it is affected by the ongoing processes in the sample during the reaction. The time dependence of $I_{o\text{-Ps}}$ indicating physical and chemical changes in the sample clearly shows three regions with different reaction kinetics, see the Fig. 4.

After the initial state of the system with slow increase of intensity, the acceleration of the curing process can be seen. The change occurs at the time of about 5000 s. A first slowdown of the crosslinking reaction was observed above 20 000 s and then the reaction was gradually terminated.

By the comparison to Fig. 2, the changes of the both parameters $\tau_{o\text{-Ps}}$ and $I_{o\text{-Ps}}$ occur at comparable times.

3.2.3. *Ortho*-positronium lifetime distribution for the different stages of curing process. The LT program also allows to evaluate the lifetime distribution. Comments and the additional figure about distributions are given in the ESI.† The



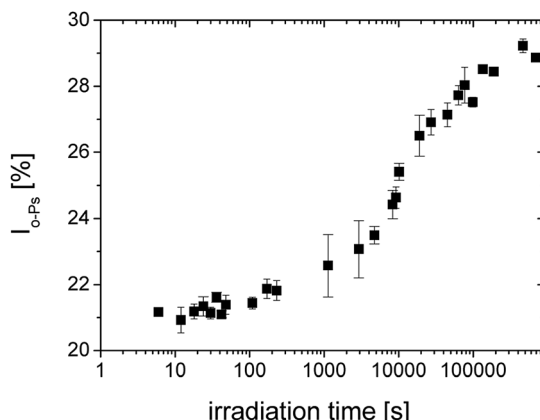


Fig. 4 The relative *o*-Ps intensity during photopolymerization of SPOT LV.

evolution of standard deviation (σ) of the lifetime distributions during photopolymerization obtained from LT program is in Fig. 5.

The width of distribution characterized by σ is a measure of homogeneity of an internal structure of the material. Fig. 5 shows the regions with unchanged distribution width, the broad peak around 1000–5000 s and then the gradual narrowing of distribution reflecting homogenization of the structure with the increasing crosslinking of the material.

Fig. 6 displays lifetime distributions for different stages of curing process given by the selected spectra with high total counts. The representative curve for the first 6 s of the irradiation time (squares, ■) considers the liquid state where the bubble effect is still present.

In this state the large width of distribution can be ascribed to the inhomogeneous system consisting of the mixture of monomers and created oligomers.

The lifetime distribution near at 5000 s of the irradiation time (circles, ●) starts to narrow and the mean lifetime shifts towards lower values. This trend was also confirmed in the length scale (Fig. S3 in ESI†).

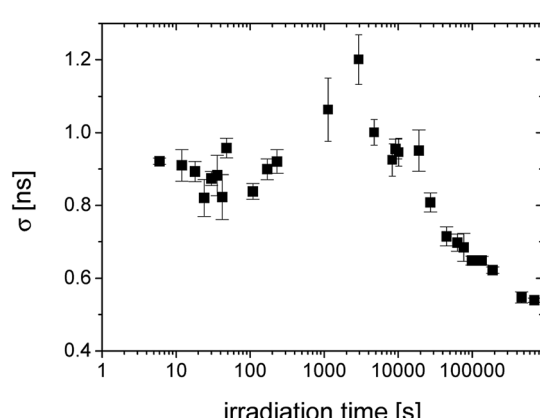


Fig. 5 The irradiation time evolution of the standard deviation of lifetime distributions (σ) given by the width of distribution.

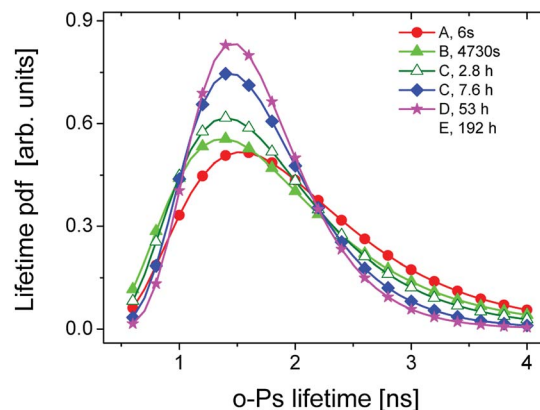


Fig. 6 The *o*-Ps lifetime distribution for different stages of network formation.

Table 1 The mean lifetime τ and the standard deviation σ of lifetime distributions determined from LT program. The analyzed distributions at given irradiation time t were selected for different stages of the curing process

t/h	τ/ns	σ/ns
0.002	2.48(0.01)	0.92(0.01)
1.3	2.32(0.04)	1.00(0.04)
2.8	2.13(0.04)	0.95(0.04)
7.6	2.00(0.04)	0.81(0.03)
53	1.83(0.01)	0.62(0.01)
192	1.77(0.01)	0.54(0.01)

The narrowing of the *o*-Ps lifetime distribution as well as the hole radius distribution can reflect the reduction of intermolecular space (free volume) due to crosslinking and the shift of lifetime/radii to lower values is attributed to the microstructural shrinkage and the reduction of the liquid phase during solidification.

In the Table 1, the mean lifetime τ and the standard deviation σ of lifetime distributions are listed for the representative spectra of various degrees of curing.

The distributions are able to reveal characteristic features of the network formation, such as appearance of crosslinked domains, homogeneity of network formation during photopolymerization that can bring more light to the understanding of the crosslinking mechanism.

From these results one can conclude that PALS is a highly sensitive technique to the different stages of reaction *via* the free volume concept. The sufficient total number of impulses in the lifetime spectrum can bring more detailed information about microstructural shrinkage and the homogeneity of the crosslinked structure.

3.2.4. A phenomenological comparison of PALS with NIR-photorheology. The phenomenological comparison of PALS response of the *o*-Ps lifetime $\tau_{o\text{-Ps}}$ (Fig. 2) and the relative intensity $I_{o\text{-Ps}}$ (Fig. 4) with the storage-, loss modulus and normal force data from photorheology (Fig. 7) confirms three distinct regions registered during the photopolymerization process. The important fact was the determination of the gel

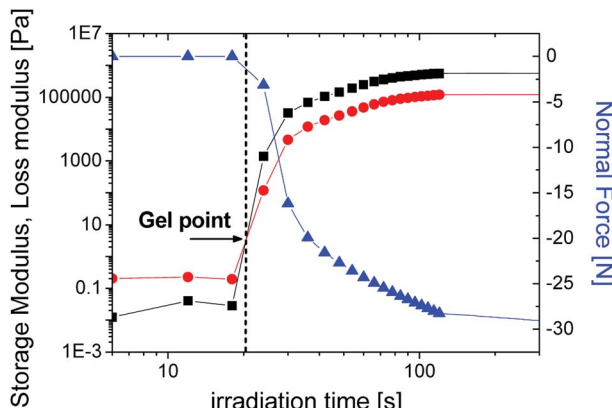


Fig. 7 The storage (■) and loss modulus (●) as well as normal force (▲) as a function of the irradiation time for SPOT LV sample.

point as an intersection point of storage and loss modulus (~ 20 s) at which the recorded shrinkage stress sharply increased (as normal force is evolving rapidly). The appearance of the gel point in PALS responses (Fig. 2, 4 and 5) can be attributed to the onset of the decrease of V_h and the increased value of $I_{o\text{-Ps}}$ accompanied with the broadening of lifetime distribution. The determination of the time for the onset of the V_h decrease is determined at 3150 ± 11 s in ESI (Fig. S4†). This value can be considered as a gel point determined for the given experimental conditions by PALS. The concomitant evolution of the double bond conversion (Fig. S5†) confirms the vitrification at low conversions (gel point observed at $\sim 20\%$), which is typical for highly crosslinking resins. The overall conversion of $>80\%$ affirms an efficient photopolymerization.

We note that the experimental conditions are not identical in PALS *versus* NIR-photorheology, due to limitations in sample thickness and for different light intensity on the surface of the sample from which follows a different irradiation time on the x -axis. These two independent sets of experiments were performed at slightly varying conditions.

In the case of distributions from the PALS, the gel point is accompanied by the broadening of the lifetime distribution. The nearest representative point from this time region with appropriate number of impulses is characterized with $\sigma = 2.32$ ns and the $\tau_{o\text{-Ps}} = 2$ ns appearing around 4730 s of irradiation time, in Fig. 6. Moreover, the KWW fit begins to increase sharply in this time region (Fig. 3).

The mutual comparison of *in situ* studies by PALS and NIR-photorheology at the phenomenological level clarifies stages of the crosslinking process and the gel point, which helps to see deeper into the underlying mechanisms.

Further optimization of experimental conditions will allow such interconnection techniques to achieve other original results important for characterization of sample properties at macro and microstructural levels. The PALS technique thus appears to be a unique tool for investigating changes in free volumes at the microstructural level even over time under defined external conditions.

4. Conclusions

In this paper, we present an *in situ* PALS study of photopolymerization on the photoresin SPOT LV. We reveal that the time evolution of the $o\text{-Ps}$ lifetime, which is proportional to the microstructural free volumes, exhibits three basic regions of the curing process with different reaction kinetics for the tested material. The nonlinear time dependence of the relative changes in the microstructural free volumes is well described by the KWW equation and is characterized by the overall time constant and the stretched exponent, which reflects shrinkage stress. Moreover, the time dependence of relative intensity $I_{o\text{-Ps}}$ shows the evolution from the liquid to crosslinked state of photopolymer. The lifetime or hole radius distributions determined from the PALS spectra reflect the reduction of intermolecular space during the curing process.

Here the gel point was ascribed to the broadening of distribution which is indicated by the intersection point of storage and loss modulus determined from photorheology. The advantage of PALS technique is in the possibility to investigate microstructural changes, *i.e.* microstructural shrinkage during photopolymerization through the free volume parameters ($\tau_{o\text{-Ps}}$, $I_{o\text{-Ps}}$) and distributions can reveal detailed features of different stages of the crosslinking process (*e.g.* gel point).

The PALS technique shows a new promising approach for a deeper understanding of network formation from the point of view of free volume and dynamic factors. These factors can lead to a reduction in the microstructural shrinkage stress, with a significant impact on the material development and the tunability of material properties.

Conflicts of interest

There are no conflicts to declare.

Acknowledgements

The authors thank the Agency VEGA Slovakia for funding project no. 2/0157/17 and the Christian Doppler Research Association and the company Ivoclar Vivadent AG for funding the framework of a Christian Doppler Laboratory for "Photopolymers in Digital and Restorative Dentistry". The financial support by the Austria Federal Ministry for Digital and Economic Affairs and the National Foundation for Research, Technology and Development is gratefully acknowledged. We also thank the following: the manufacturer Sonnaya Ulitka S.L., DIVISION Spot-A Materials, Barcelona, Spain, for providing information about the sample; the firm Edico Sk, Bratislava, Slovakia, for technical consultations and for giving samples; Ing. Vojtech Nádaždy, CSc., at the Institute of Physics, Slovak Academy of Science, Bratislava, Slovakia, for the flux density measurements of the light sources.

References

- Y. Abe, *DIC Tech. Rev.*, 2005, **11**, 1–20.



2 C. Dworak, T. Koch, F. Varga and R. Liska, *J. Polym. Sci., Part A: Polym. Chem.*, 2010, **48**, 2916–2924.

3 J. TorgerSEN, X.-H. Qin, Z. Li, A. Ovsianikov, R. Liska and J. Stampfl, *Adv. Funct. Mater.*, 2013, **23**, 4542–4554.

4 K. S. Anseth, C. N. Bowman and N. A. Peppas, *J. Polym. Sci., Part A: Polym. Chem.*, 1994, **32**, 139–147.

5 F. Catalina, C. Peinado, R. Sastre, J. L. Mateo and N. S. Allen, *J. Photochem. Photobiol. A*, 1989, **47**, 365–377.

6 V. Y. Voytekunas, F. L. Ng and M. J. M. Abadie, *Eur. Polym. J.*, 2008, **44**, 3640–3649.

7 C. Decker and K. Moussa, *Makromol. Chem.*, 1988, **189**, 2381–2394.

8 C. Decker and K. Moussa, *J. Coat. Technol.*, 1990, **36**(786), 55–61.

9 C. Gorsche, R. Harikrishna, S. Baudis, P. Knaack, B. Husar, J. Laeuger, H. Hoffmann and R. Liska, *Anal. Chem.*, 2017, **89**, 4958–4968.

10 A. Botella, J. Dupuy, A. A. Roche, H. Sautereau and V. Verney, *Macromol. Rapid Commun.*, 2004, **25**, 1155–1158.

11 I. Alig, D. Lellinger, S. Agarwal and H. Oehler, *React. Funct. Polym.*, 2013, **73**, 316–322.

12 Y. Lin and J. W. Stansbury, *RadTech e/5, Technical Proceedings*, 2004.

13 D. Schuele, R. Renner and D. Coleman, *Mol. Cryst. Liq. Cryst.*, 1997, **299**, 343–352.

14 K. Zahouily, C. Decker, E. Kaisersberger and M. Gruener, *Eur. Coat. J.*, 2003, **11**, 14–18.

15 H. Lu, J. W. Stansbury and C. N. Bowman, *Dent. Mater.*, 2004, **20**, 979–986.

16 R. R. Braga, R. Y. Ballester and J. L. Ferrance, *Dent. Mater.*, 2005, **21**, 962–970.

17 L. F. J. Schneider, L. M. Cavalcante and N. Silikas, *J. Dent. Biomech.*, 2010, **1**, 1–14.

18 C. E. Hoyle and C. N. Bowman, *Angew. Chem., Int. Ed.*, 2010, **49**(9), 1540–1573.

19 G. Moad, E. Rizzardo and S. H. Thang, *Polymer*, 2008, **49**(5), 1079–1131.

20 K. Seidler, M. Griesser, M. Kury, H. Reghunathan, P. Dorfinger, T. Koch, A. Svirkova, M. Marchetti-Deschmann, J. Stampfl, N. Moszner, C. Gorsche and R. Liska, *Angew. Chem., Int. Ed.*, 2018, **57**, 9165–9169.

21 C. Gorsche, T. Koch, N. Moszner and R. Liska, *Polym. Chem.*, 2015, **6**, 2038–2047.

22 T. Goworek, *Annales Universitatis Mariae Curie-Sklodowska*, 2014, **69**, 1–110.

23 H. Švajdlenková, O. Šauša, J. Steindl, T. Koch and C. Gorsche, *J. Polym. Sci., Part B: Polym. Phys.*, 2016, **54**, 2476–2484.

24 H. Švajdlenková, O. Šauša, I. Matko, T. Koch and C. Gorsche, *Macromol. Chem. Phys.*, 2018, **219**, 1800119.

25 V. Majerník, J. Krištiak, O. Šauša and M. Iskrová-Miklošovičová, *Mater. Sci. Forum*, 2013, **733**, 84–87.

26 N. García-Huete, E. Axpe, J. M. Cuevas, D. Merida, J. M. Laza, J. A. García, J. L. Vilas, F. Plazaola and L. M. Leon, *Polymer*, 2017, **109**, 66–70.

27 K. Krzemien, J. Kansy and J. E. Frackowiak, *Acta Phys. Pol. A*, 2005, **107**, 837–841.

28 T. Hirade, F. H. J. Maurer and M. Eldrup, *Radiat. Phys. Chem.*, 2000, **58**, 465–471.

29 T. Goworek, B. Zgierzinska, M. Pietrow and J. Wawryszczuk, *Mater. Sci. Forum*, 2013, **733**, 67–74.

30 M. Pietrow and J. Wawryszczuk, *Mater. Sci. Forum*, 2013, **733**, 75–79.

31 A. J. Hill, *AIP Conf. Proc.*, 1999, **497**, 699–705.

32 J. Kanzow, V. Zaporotchenko, H. Nabika, M. Mizuhata, S. Deki and F. Faupel, *Mater. Sci. Forum*, 2004, **445–446**, 313–315.

33 M. Hyla, J. Filipecki, J. Swiatek, R. I. Mervinskii, L. A. Gudzowska and V. Savitsky, *J. Non-Cryst. Solids*, 2001, **290**, 20–24.

34 J. Filipecki, K. Chamerski, O. Boyko and K. Kotynia, *Polim. Med.*, 2014, **44**(1), 21–28.

35 O. Shpotyuk, S. Adamiak, E. Bezwushko, J. Cebulski, M. Iskiv, O. Shpotyuk and V. Balitska, *Nanoscale Res. Lett.*, 2017, **12**, 75.

36 http://spotamaterials.com/wp/wp-content/uploads/2015/07/Spot-LV_MSDS_tmp.pdf.

37 J. Kansy, *Nucl. Instrum. Methods Phys. Res., Sect. A*, 1996, **374**, 235–244.

38 M. Eldrup, D. Lightbody and J. N. Sherwood, *Chem. Phys.*, 1981, **63**, 51–58.

39 S. J. Tao, *J. Chem. Phys.*, 1972, **56**, 5499–5510.

40 H. Nakanishi, S. Wang and Y. Jean, Microscopic surface tension studies by positron annihilation, in *Int. Symp. Positron Annihil. Stud. Fluids*, ed. S.C. Sharma, World Scientific Publishing, Singapore, 1988, p. 292.

41 G. Williams and D. C. Watts, *Trans. Faraday Soc.*, 1970, **66**, 80–85.

42 R. A. Ferrell, *Phys. Rev.*, 1957, **108**, 167–175.

43 B. Zgierzinska, *Mater. Sci. Forum*, 2013, **733**, 29–32.

44 J. F. Kincaid and H. Eyring, *J. Chem. Phys.*, 1938, **6**, 620–629.

45 R. Zaleski, J. Goworek and M. Maciejewska, *Phys. Status Solidi C*, 2009, **6**, 2445–2447.

46 C. He, B. Xiong, W. Mao, Y. Kobayashi, T. Oka, N. Oshima and R. Suzuki, *Chem. Phys. Lett.*, 2013, **590**, 97–100.

